

# The influence of metal oxide additives on the molecular structures of surface tungsten oxide species on alumina: I. Ambient conditions

Marlene M. Ostromecki<sup>a</sup>, Loyd J. Burcham<sup>a</sup>, Israel E. Wachs<sup>a,\*</sup>,  
Narayanan Ramani<sup>b</sup>, John G. Ekerdt<sup>b</sup>

<sup>a</sup> Zettlemoyer Center for Surface Studies, and Department of Chemical Engineering, Lehigh University, Bethlehem, PA 18015, USA

<sup>b</sup> Department of Chemical Engineering, The University of Texas at Austin, Austin, TX 78712, USA

Received 25 June 1997; accepted 9 October 1997

## Abstract

The molecular structures of  $\text{WO}_3/\text{Al}_2\text{O}_3$  catalysts, with and without the presence of secondary metal oxide additives (P, Sn, Fe, Ni, Zn, Ce, Co, La, Ca, Mg, K and Na), were determined with Raman spectroscopy under ambient conditions where the surface is hydrated. The hydrated surface tungsten oxide species found on the alumina support ( $\text{WO}_4^{2-}$ ,  $\text{HW}_6\text{O}_{21}^{5-}$ , and U-metatungstate) were related to the net pH at the point of zero charge (pzc) of the thin aqueous layer. The isolated tungstate species was dominant at high pH values and the polytungstate species were dominant at lower pH values. The net pH at pzc was a function of tungsten oxide loading (decreasing from 8.9 to 4.4 for 1 to 25%  $\text{WO}_3/\text{Al}_2\text{O}_3$ , respectively) and the specific secondary metal oxide additive ( $\text{Na} > \text{K} > \text{Mg} > \text{Ca} > \text{La} > \text{Co} > \text{Ce} > \text{Zn} > \text{Ni} > \text{Fe} > \text{Sn} > \text{P}$ ). Below monolayer coverages, the secondary metal oxide additives preferentially interacted with the alumina support to form surface metal oxide species rather than with the tungsten oxide species to form mixed tungsten oxide crystalline compounds. Above monolayer coverages, both surface metal oxide species and mixed tungsten oxide crystalline compounds were formed. The more basic secondary metal oxide additives (Ca, La) formed mixed tungsten oxide crystalline compounds. In the absence of the formation of mixed tungsten oxide crystalline compounds, the alumina support was able to accommodate approximately two monolayer-equivalents of the surface metal oxides during calcination because the surface tungsten oxide species and the secondary surface metal oxide species occupied different sites on the alumina support. The surface tungsten oxide species preferentially interacted with the surface hydroxyls of the alumina support and the secondary surface metal oxide species preferentially interacted with coordinately unsaturated  $\text{Al}^{+3}$  sites. © 1998 Elsevier Science B.V. All rights reserved.

**Keywords:** Tungsten oxide; Secondary metal oxide additives; Ambient Raman spectroscopy

## 1. Introduction

Alumina supported tungsten oxide catalysts, which are used for hydrocarbon cracking and

hydrotreating reactions [1–5], usually contain various additives that are intentionally or unintentionally added. NiO, CoO, and  $\text{P}_2\text{O}_5$  are used as promoters for hydrotreating reactions [6].  $\text{Fe}_2\text{O}_3$  acts as a poison and is deposited during petroleum processing. The additives MgO,  $\text{SnO}_2$ ,  $\text{La}_2\text{O}_3$ ,  $\text{CeO}_2$ , and ZnO act as passivat-

\* Corresponding author. Tel.: +1-610-7584539; fax: +1-610-7586555; e-mail: gd00@lehigh.edu

ing agents to mitigate the effects of feed poisons such as  $\text{Fe}_2\text{O}_3$  and  $\text{V}_2\text{O}_5$ . In addition,  $\text{K}_2\text{O}$ ,  $\text{Na}_2\text{O}$  and  $\text{CaO}$  may be inadvertently introduced during the catalyst preparation or processing of the alumina support [7–10]. Despite this widespread presence of additives, however, very few fundamental studies have been performed on the influence of additives upon alumina supported tungsten oxide catalysts [11,12].

In general, supported metal oxide catalysts, such as alumina supported tungsten oxide, primarily contain the active metal oxide as a two-dimensional metal oxide overlayer on the alumina support [13]. Under ambient conditions, these catalysts, including both unpromoted and promoted  $\text{WO}_3/\text{Al}_2\text{O}_3$  systems, contain a thin film of water that hydrates the surface metal oxide species ( $\sim 8$  wt%  $\text{H}_2\text{O}$  [14]). Horsley et al. [15] demonstrated with Raman spectroscopy and X-ray absorption near edge spectroscopy (XANES) that at low surface tungsten oxide coverages ( $< 1/3$  monolayer), a hydrated  $\text{WO}_4$  species is primarily present. At higher surface coverages, a hydrated octahedrally coordinated cluster, which best matches the structure of  $\text{W}_{12}\text{O}_{39}$  [16], is present on the alumina surface. Raman spectroscopy is widely used to discriminate between different metal oxide molecular structures because of its in situ capabilities, ease of data acquisition, and compatibility with many different supported metal oxide systems [12,13].

More recent studies have shown that the hydrated molecular structure of surface metal oxide species on oxide supports are determined by the net pH at pzc (point of zero charge) of the

thin aqueous layer [14,17]. The net pH at pzc of a supported metal oxide catalyst under ambient conditions is determined by the specific oxide support and surface coverages of the specific metal oxide overlayers. Furthermore, comparison of the Raman bands of the hydrated surface metal oxide species on alumina with the corresponding aqueous metal oxide species reveals that essentially the same metal oxide species are present in both systems. This suggests that the hydrated surface metal oxide species are not anchored to the oxide support under ambient conditions, but are suspended in the thin aqueous layer.

In pure aqueous solutions, the specific tungsten oxide species that can exist depend on the solution pH and the tungsten oxide concentration. The various aqueous phase tungsten oxide species and their corresponding Raman bands [18] are listed in Table 1. These Raman bands were approximated from Raman spectra presented in Ref. [18], and have an error of approximately  $\pm 5$   $\text{cm}^{-1}$  since the exact Raman band positions were not reported. It was difficult to determine the positions of Raman bands below  $\sim 300$   $\text{cm}^{-1}$  because of the presence of strong Rayleigh scattering in the spectra. The isopolytungstate ions in aqueous solution were formed by the acidification of monotungstate solutions between 0.2 and 2 M. However, reports in the literature have not agreed upon the exact pH values at which each of the isopolytungstate ions exist in solution [18–21]. The general agreement is that the monotungstate ion ( $\text{WO}_4^{-2}$ ) exists at pH values of greater than  $\sim 7.5$ , the

Table 1  
Raman bands for various aqueous tungstate ions, approximated from [18]

Isopolytungstate ions	Raman bands ( $\text{cm}^{-1}$ )
Monotungstate $\text{WO}_4^{-2}$	932(s), 834(w), 330(m)
Para-A-tungstate $\text{HW}_6\text{O}_{21}^{-5}$	962(s), 901(m), 650(w), 360(w), 300(w)
Para-B-tungstate $\text{HW}_{12}\text{O}_{42}^{-10}$	955(s), 880(w), 830(w), 650(w), 360(w), 300(w)
U-metatungstate (no formula)	969(s), 900(w), 650(w), 360(w)
Metatungstate $\text{H}_2\text{W}_{12}\text{O}_{40}^{-6}$	978(s), 961(s), 900(w), 650(w)
Polytungstate-Y $\text{W}_{10}\text{O}_{32}^{-4}$	988(s), 972(s), 900(w), 830(w), 600(w), 400(w)

(s) = strong, (m) = medium, (w) = weak, all wavenumbers approximated from Ref. [18].

paratungstate-A ( $\text{HW}_6\text{O}_{21}^{-5}$ ) and paratungstate-B ions ( $\text{H}_2\text{W}_{12}\text{O}_{40}^{-6}$ ) exist at pH values of  $\sim 4.5$ – $7.5$ , the U metatungstate ion (structural formula unknown) exists at pH values of  $\sim 3$ – $4$ , and the metatungstate ( $\text{HW}_{12}\text{O}_{42}^{-10}$ ) and polytungstate-Y ions ( $\text{W}_{10}\text{O}_{32}^{-4}$ ) exist at pH values of  $\sim 1$ – $3$  for  $0.1$  to  $1$  M acidified monotungstate solutions. The concentrations of the isopolytungstate ions in aqueous solution, however, is also a critical parameter [17].

Raman band assignments can be made based on the fact that the local structure of the isopolytungstates are made up of  $\text{WO}_6$  octahedra while the monotungstate ion consists of  $\text{WO}_4$  tetrahedra [22,23]. For the polytungstate ions, the Raman bands above  $900\text{ cm}^{-1}$  are attributed to  $\text{W}=\text{O}$  stretches within  $\text{WO}_6$  species, bands near  $350\text{ cm}^{-1}$  are the corresponding bending modes of these  $\text{WO}_6$  species, bands in the  $800$ – $900\text{ cm}^{-1}$  range are due to symmetric  $\text{O}-\text{W}-\text{O}$  stretches, bands in the  $600$ – $400\text{ cm}^{-1}$  range are assigned to  $\text{W}-\text{O}-\text{W}$  symmetric stretches, and bands near  $200\text{ cm}^{-1}$  are due to  $\text{W}-\text{O}-\text{W}$  bending modes [16,24]. For the monotungstate ion, there are no vibrations due to  $\text{W}-\text{O}-\text{W}$  linkages and the Raman bands at  $932$ ,  $834$ , and  $330\text{ cm}^{-1}$  are due to the symmetric stretch, antisymmetric stretch, and bending mode of  $\text{WO}_4$  species, respectively [24]. The Raman band due to the symmetric stretch of the terminal  $\text{W}=\text{O}$  bond of the aqueous tungsten ions systematically increases in frequency with decreasing solution pH (see Table 1). Finally, there exists an additional possibility of forming heteropolytungstate anions (e.g.  $\text{PW}_{12}\text{O}_{40}^{-3}$ , known as the Keggin structure) when secondary metal cations are present in acidic aqueous solutions of isopolytungstate ions [25], but much less is known about the phase behavior of heteropolytungstates.

The objective of this investigation was to determine the specific surface tungsten oxide species present in both  $\text{WO}_3/\text{Al}_2\text{O}_3$  catalysts and upon the addition of secondary metal oxides to  $\text{WO}_3/\text{Al}_2\text{O}_3$  catalysts under ambient conditions. The influence of a wide variety of metal

oxide additives upon the molecular structure of the surface tungsten oxide species on alumina was of particular interest. The molecular structures of the surface tungsten oxide species were determined with Raman spectroscopy and the net pH at pzc values were experimentally determined by the mass titration method [14]. The surface tungsten oxide coverage on the alumina support was varied from  $0.036$  to  $0.9$  monolayer (corresponding to  $1$ – $25$  wt%  $\text{WO}_3/\text{Al}_2\text{O}_3$  or  $0.14$ – $3.6$  W atoms/ $\text{nm}^2$ ). The secondary metal oxides were added to  $10\%$   $\text{WO}_3/\text{Al}_2\text{O}_3$  ( $0.36$  monolayer coverage) and  $25\%$   $\text{WO}_3/\text{Al}_2\text{O}_3$  ( $0.9$  monolayer coverage) in equal molar amounts to form promoted  $\text{WO}_3/\text{Al}_2\text{O}_3$  catalysts possessing  $\sim 0.7$  and  $\sim 1.8$  monolayer-equivalents coverage on the alumina support (one monolayer-equivalent surface coverage corresponds to depositing  $4.0$  metal oxide atoms/ $\text{nm}^2$  of alumina).

## 2. Experimental

### 2.1. Sample preparation

The alumina support used in this study was obtained from Harshaw ( $180\text{ m}^2/\text{g}$ ). The  $\text{WO}_3/\text{Al}_2\text{O}_3$  samples were prepared by incipient wetness impregnation with an aqueous solution of ammonium metatungstate (Pfaltz and Bauer). After impregnation, the samples were initially dried at room temperature overnight, further dried at  $120^\circ\text{C}$  overnight, and calcined in dry air at  $500^\circ\text{C}$  overnight.

The secondary metal oxide/ $\text{WO}_3/\text{Al}_2\text{O}_3$  samples were prepared by subsequently adding secondary metal oxides ( $\text{SnO}_2$ ,  $\text{P}_2\text{O}_5$ ,  $\text{CeO}_2$ ,  $\text{Fe}_2\text{O}_3$ ,  $\text{ZnO}$ ,  $\text{CoO}$ ,  $\text{NiO}$ ,  $\text{La}_2\text{O}_3$ ,  $\text{MgO}$ ,  $\text{CaO}$ ,  $\text{Na}_2\text{O}$  and  $\text{K}_2\text{O}$ ) to the  $\text{WO}_3/\text{Al}_2\text{O}_3$  samples. The secondary metal oxides  $\text{P}_2\text{O}_5$ ,  $\text{CeO}_2$ ,  $\text{Fe}_2\text{O}_3$ ,  $\text{ZnO}$ ,  $\text{CoO}$ ,  $\text{NiO}$ ,  $\text{La}_2\text{O}_3$ ,  $\text{MgO}$ ,  $\text{CaO}$ ,  $\text{Na}_2\text{O}$  and  $\text{K}_2\text{O}$  were added by incipient wetness impregnation of aqueous solutions of  $85\%$  w/w phosphoric acid (Fisher Scientific), cerium (III) nitrate (Johnson Matthey), iron (III) nitrate (Alfa

Aesar), zinc acetate reagent (Alfa Products), cobalt (II) acetate (Alfa Aesar), nickelous nitrate 6-hydrate (Baker Chemical), lanthanum nitrate hexahydrate (Aldrich Chemical), magnesium acetate 4-hydrate (Johnson Matthey), calcium nitrate hydrate (Aldrich Chemical), 50% w/w sodium hydroxide solution (Fisher Scientific), and 45% w/w potassium hydroxide solution (Fisher Scientific), respectively. After impregnation of the secondary metal oxides, the samples were initially dried at room temperature overnight, further dried at 120°C overnight, and finally calcined in dry air at 500°C overnight.

The secondary metal oxide SnO<sub>2</sub> was added by incipient wetness impregnation with a solution of 10% w/v of tin isopropoxide (Johnson Matthey) in isopropanol. The impregnation, subsequent drying at room temperature overnight, and heating at 120°C overnight were performed in a nitrogen atmosphere due to the air and moisture sensitivity of this alkoxide precursor. The samples were finally calcined in nitrogen at 500°C overnight.

## 2.2. Raman characterization studies

The Raman spectrometer system used in this study consisted of a Triplemate spectrometer (Spex, Model 1877) coupled to an optical multi-channel analyzer (Princeton Applied Research model 1463) equipped with an intensified photodiode array detector (cooled to -35°C). The samples were analyzed under ambient conditions as pressed wafers of ~150 mg and the argon ion laser (Spectra Physics) was focused onto the spinning sample wafer (Sample Rotator: SPEX, Model 1445A). The 514.5 nm line of the laser was used as the excitation source. The laser power at the sample was 15–40 mW. The acquisition time used per scan was 30 s and 25 scans were averaged. The spectrometer resolution was approximately 2 cm<sup>-1</sup>.

## 2.3. Net pH at PZC measurements

The net pH at pzc values of the unsupported secondary metal oxides and tungsten oxide were

calculated from formulas proposed by Butler et al. [26] and Parks [27]. The net pH at pzc values of the WO<sub>3</sub>/Al<sub>2</sub>O<sub>3</sub> and secondary metal oxide/WO<sub>3</sub>/Al<sub>2</sub>O<sub>3</sub> monolayer catalysts were measured by the mass titration method [14]. A 0.1 M NaCl solution was prepared using distilled, deionized, and degassed water. Various amounts of solid samples were added to a series of Erlenmeyer flasks and sealed. The flasks were evacuated and backfilled with nitrogen. The NaCl solution was transferred to the flasks under a nitrogen atmosphere. The oxide catalysts/water solutions were stirred overnight with a magnetic stirrer. The pH of each solution was measured with a standard pH meter after 24 h of stirring. The pH meter was calibrated with commercial buffer solutions of pH 7, and either pH 4 or pH 10 before each measurement.

## 3. Results

### 3.1. WO<sub>3</sub>/Al<sub>2</sub>O<sub>3</sub> catalysts

#### 3.1.1. Raman spectra

The Raman spectra of the hydrated WO<sub>3</sub>/Al<sub>2</sub>O<sub>3</sub> catalysts are presented in Fig. 1 as a function of tungsten oxide coverage. The 1% WO<sub>3</sub>/Al<sub>2</sub>O<sub>3</sub> (0.036 monolayer coverage) catalyst has a broad and weak Raman band at ~951 cm<sup>-1</sup>, as well as much weaker Raman bands at ~880 and ~330 cm<sup>-1</sup>. The 951 cm<sup>-1</sup> band is due to the symmetric stretch of the W=O bond within distorted WO<sub>4</sub> species, while the ~330 cm<sup>-1</sup> band is due to the bending mode of these distorted WO<sub>4</sub> species [15,16]. As the tungsten oxide loading is increased to 25% (0.9 monolayer coverage) additional weak Raman bands appear at ~580 and ~210 cm<sup>-1</sup>, which are due to the symmetric stretching and bending of polymeric W–O–W linkages, respectively [15,16]. Also, the Raman band due to the symmetric stretch of the W=O bond sharpens and shifts to 975 cm<sup>-1</sup> (as the ratio of WO<sub>6</sub> to WO<sub>4</sub> increases with the forma-

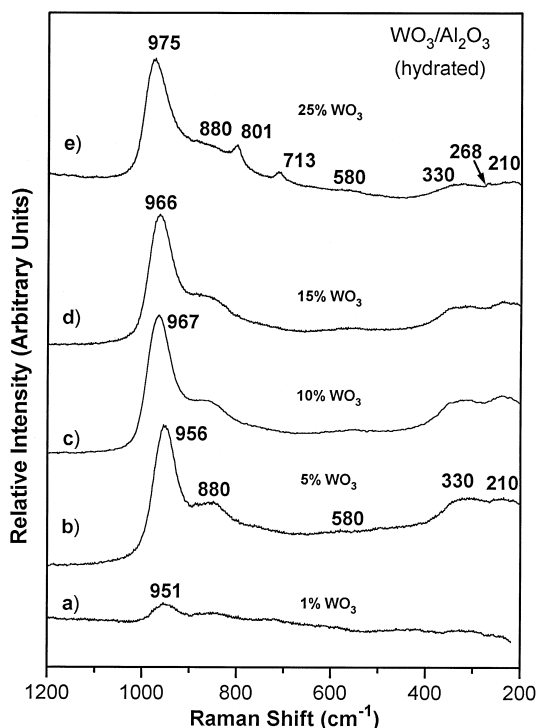


Fig. 1. Hydrated  $\text{WO}_3/\text{Al}_2\text{O}_3$  catalysts.

tion of polytungstate structures [22–24]). The broad band at  $\sim 880\text{ cm}^{-1}$  has been assigned by Vuurman et al. [11,16] as the symmetric stretch of O–W–O polymeric linkages for the higher loadings. This is consistent with the fact that other bands associated with polymeric linkages are also observed in these spectra at  $\sim 580$  and  $\sim 210\text{ cm}^{-1}$ . However, at the lowest loading (1%  $\text{WO}_3/\text{Al}_2\text{O}_3$ ), the very weak band at  $\sim 880\text{ cm}^{-1}$  is probably due to the asymmetric stretch of isolated  $\text{WO}_4$  tetrahedra, since this mode is also expected to be in this region of the spectrum and there are no other polymeric bands

at  $\sim 580$  or  $\sim 210\text{ cm}^{-1}$  [15]. The small Raman bands at 801, 713, and  $268\text{ cm}^{-1}$  for the 25%  $\text{WO}_3/\text{Al}_2\text{O}_3$  (0.9 monolayer coverage) catalyst are characteristic of trace amounts of undispersed microcrystalline  $\text{WO}_3$  particles [28,29]. The Raman bands of crystalline  $\text{WO}_3$  particles become very pronounced above 28%  $\text{WO}_3/\text{Al}_2\text{O}_3$  (1.0 monolayer coverage) since monolayer coverage is exceeded (not shown in Fig. 1).

### 3.1.2. Net pH at pzc measurements

The net surface pH at pzc measurements of the  $\text{WO}_3/\text{Al}_2\text{O}_3$  catalysts are listed in Table 2 and reveal a decreasing net surface pH at pzc with increasing surface tungsten oxide coverage. Thus, the net surface pH at pzc of a catalyst is dependent on the coverage of the surface metal oxide species on the alumina support.

### 3.2. Secondary metal oxide / $\text{WO}_3/\text{Al}_2\text{O}_3$ catalysts

The Raman spectra of the 0.7 monolayer-equivalent hydrated secondary metal oxide/ $\text{WO}_3/\text{Al}_2\text{O}_3$  catalysts are compared to the Raman spectrum of the unpromoted, hydrated 10%  $\text{WO}_3/\text{Al}_2\text{O}_3$  catalyst in Fig. 2-1 through Fig. 2-3. The Raman spectra of the 1.8 monolayer-equivalents hydrated secondary metal oxide/ $\text{WO}_3/\text{Al}_2\text{O}_3$  catalysts are compared to the Raman spectrum of the unpromoted, hydrated 25%  $\text{WO}_3/\text{Al}_2\text{O}_3$  catalyst in Fig. 3-1 through Fig. 3-3. The Raman spectra of the promoted  $\text{WO}_3/\text{Al}_2\text{O}_3$  samples are dominated

Table 2  
Net surface pH at the point of zero charge for  $\text{WO}_3/\text{Al}_2\text{O}_3$  catalysts

Catalyst	Net pH at point of zero charge (pzc)
1% $\text{WO}_3/\text{Al}_2\text{O}_3$ (0.036 monolayer coverage)	7.45
5% $\text{WO}_3/\text{Al}_2\text{O}_3$ (0.18 monolayer coverage)	7.15
10% $\text{WO}_3/\text{Al}_2\text{O}_3$ (0.36 monolayer coverage)	6.06
15% $\text{WO}_3/\text{Al}_2\text{O}_3$ (0.54 monolayer coverage)	5.72
25% $\text{WO}_3/\text{Al}_2\text{O}_3$ (0.90 monolayer coverage)	4.38

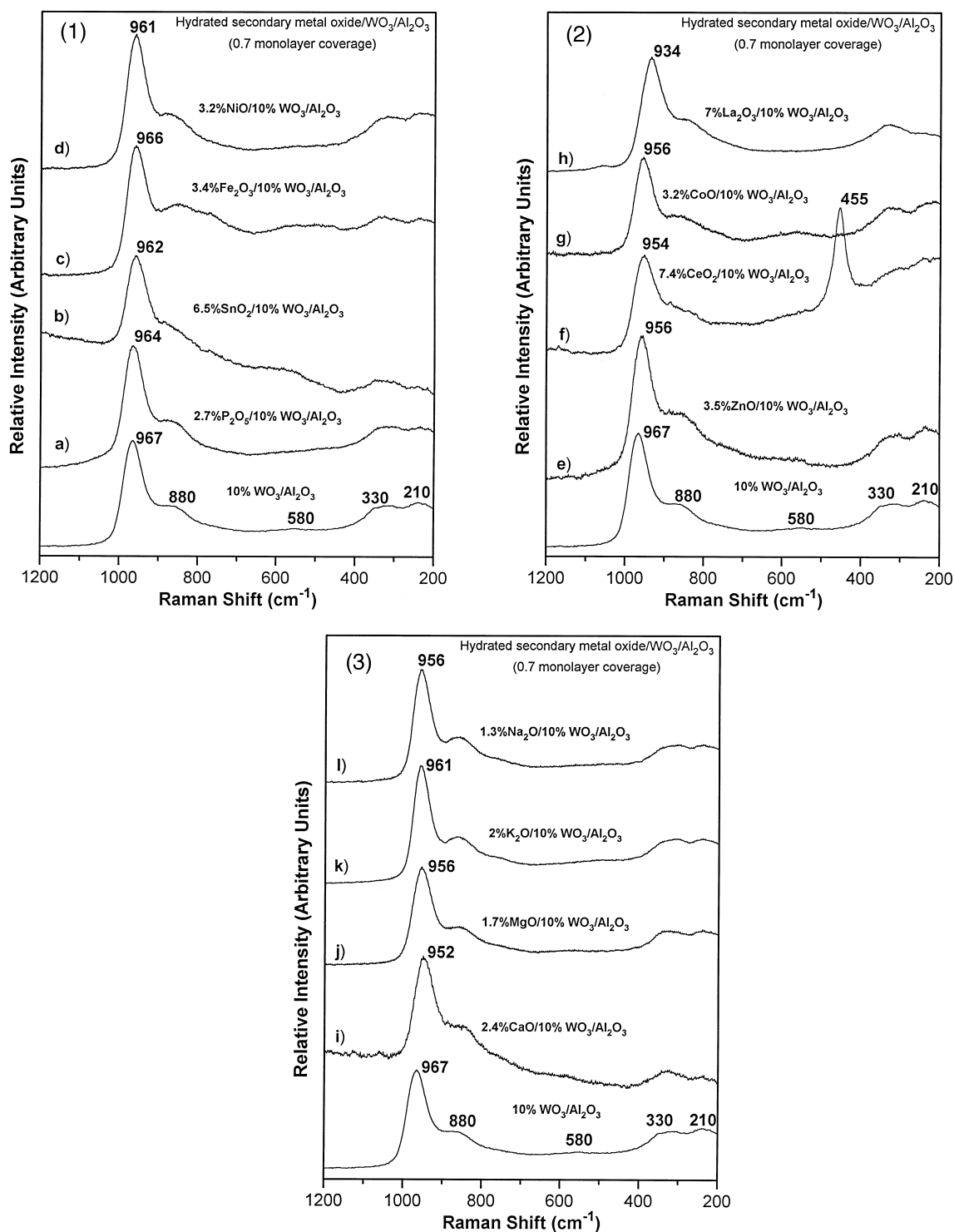


Fig. 2. (1) (a) 2.7%  $\text{P}_2\text{O}_5/10\% \text{WO}_3/\text{Al}_2\text{O}_3$  (b) 6.5%  $\text{SnO}_2/10\% \text{WO}_3/\text{Al}_2\text{O}_3$  (c) 3.4%  $\text{Fe}_2\text{O}_3/10\% \text{WO}_3/\text{Al}_2\text{O}_3$  (d) 3.2%  $\text{NiO}/10\% \text{WO}_3/\text{Al}_2\text{O}_3$ ; (2) (e) 3.5%  $\text{ZnO}/10\% \text{WO}_3/\text{Al}_2\text{O}_3$  (f) 3.2%  $\text{CoO}/10\% \text{WO}_3/\text{Al}_2\text{O}_3$  (g) 7.4%  $\text{CeO}_2/10\% \text{WO}_3/\text{Al}_2\text{O}_3$  (h) 7%  $\text{La}_2\text{O}_3/10\% \text{WO}_3/\text{Al}_2\text{O}_3$ ; (3) (i) 2.5%  $\text{CaO}/10\% \text{WO}_3/\text{Al}_2\text{O}_3$  (j) 1.7%  $\text{MgO}/10\% \text{WO}_3/\text{Al}_2\text{O}_3$  (k) 2%  $\text{K}_2\text{O}/10\% \text{WO}_3/\text{Al}_2\text{O}_3$  (l) 1.3%  $\text{Na}_2\text{O}/10\% \text{WO}_3/\text{Al}_2\text{O}_3$ .

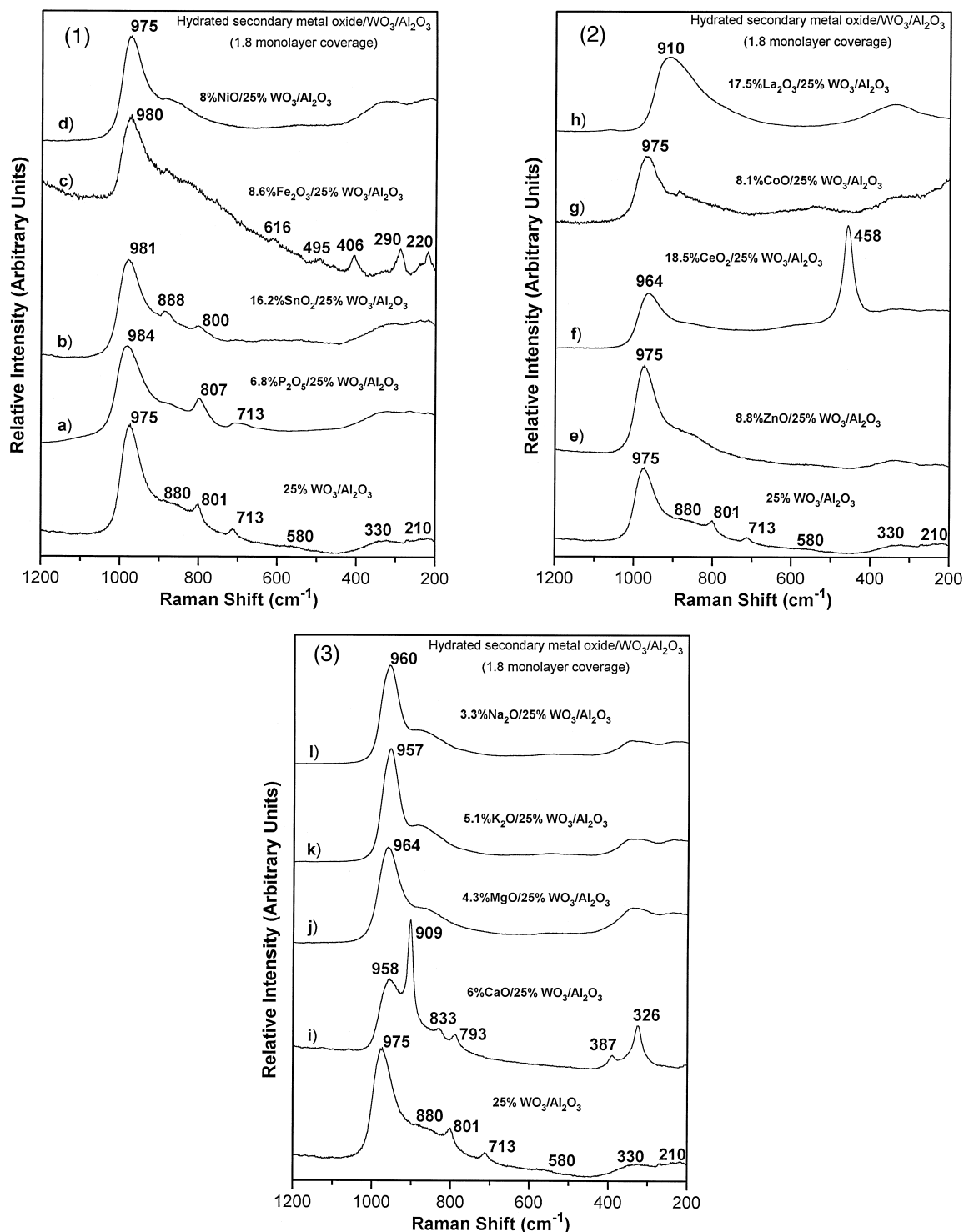


Fig. 3. (1) (a) 6.8%  $\text{P}_2\text{O}_5$ /25%  $\text{WO}_3/\text{Al}_2\text{O}_3$  (b) 16%  $\text{SnO}_2$ /25%  $\text{WO}_3/\text{Al}_2\text{O}_3$  (c) 8.6%  $\text{Fe}_2\text{O}_3$ /25%  $\text{WO}_3/\text{Al}_2\text{O}_3$  (d) 8%  $\text{NiO}$ /25%  $\text{WO}_3/\text{Al}_2\text{O}_3$ ; (2) (e) 8.8%  $\text{ZnO}$ /25%  $\text{WO}_3/\text{Al}_2\text{O}_3$  (f) 8%  $\text{CoO}$ /25%  $\text{WO}_3/\text{Al}_2\text{O}_3$  (g) 18.5%  $\text{CeO}_2$ /25%  $\text{WO}_3/\text{Al}_2\text{O}_3$  (h) 17.5%  $\text{La}_2\text{O}_3$ /25%  $\text{WO}_3/\text{Al}_2\text{O}_3$ ; (3) (i) 6%  $\text{CaO}$ /25%  $\text{WO}_3/\text{Al}_2\text{O}_3$  (j) 4.3%  $\text{MgO}$ /25%  $\text{WO}_3/\text{Al}_2\text{O}_3$  (k) 5%  $\text{K}_2\text{O}$ /25%  $\text{WO}_3/\text{Al}_2\text{O}_3$  (l) 3.3%  $\text{Na}_2\text{O}$ /25%  $\text{WO}_3/\text{Al}_2\text{O}_3$ .

by the tungsten oxide vibrational modes because the secondary metal oxide surface species have much weaker Raman scattering cross-sections than those of tungsten–oxygen bonds [30,31]. As a result, the Raman spectra of the promoted samples provide direct information on the tungsten oxide surface species, but only indirect information about the secondary metal oxides through their effect on the tungsten oxide surface species (e.g., shifts in the W=O band position and formation of crystalline compounds). Furthermore, the W=O symmetric stretching mode is generally the most frequency-sensitive Raman band to changes in the molecular structures of surface tungsten oxide species due to its sharpness and intensity. However, changes in the other bands at  $\sim 880$ ,  $\sim 580$ ,  $\sim 330$ , and  $\sim 210$   $\text{cm}^{-1}$  will be discussed in cases where they are significantly different from the unpromoted  $\text{WO}_3/\text{Al}_2\text{O}_3$ .

At submonolayer loadings (0.7 monolayer-equivalent), the frequency of the W=O symmetric stretch in the Raman spectra of catalysts promoted by the secondary metal oxides  $\text{P}_2\text{O}_5$ ,  $\text{SnO}_2$ , and  $\text{Fe}_2\text{O}_3$  (Fig. 2-1, a–c) is within 5  $\text{cm}^{-1}$  of the frequency for this mode in the original, unpromoted 10%  $\text{WO}_3/\text{Al}_2\text{O}_3$  catalyst at 967  $\text{cm}^{-1}$ . The Raman spectra of samples promoted by the other secondary metal oxides (NiO, ZnO,  $\text{CeO}_2$ , CoO,  $\text{La}_2\text{O}_3$ , CaO, MgO,  $\text{K}_2\text{O}$ , and  $\text{Na}_2\text{O}$ ; see Fig. 2-1 through Fig. 2-3, d–l) exhibit a downshift of the W=O symmetric stretching frequency by  $\sim 6$ –15  $\text{cm}^{-1}$ , which corresponds to a lengthening of the W=O bond length relative to the unpromoted 10%  $\text{WO}_3/\text{Al}_2\text{O}_3$  catalyst [15,32]. An exception to these trends is  $\text{La}_2\text{O}_3$ , which lowers the frequency of the W=O symmetric stretch by 33  $\text{cm}^{-1}$ , along with a change in the general shape of the spectrum relative to unpromoted  $\text{WO}_3/\text{Al}_2\text{O}_3$  (see Fig. 2-2, h). As will be discussed below, compound formation between  $\text{La}_2\text{O}_3$  and the tungsten oxide surface species is responsible for this behavior. Crystalline  $\text{CeO}_2$  particles (Raman band at 455  $\text{cm}^{-1}$  [33]) are also present on the 7.4%  $\text{CeO}_2/10\%$

$\text{WO}_3/\text{Al}_2\text{O}_3$  catalyst (see Fig. 2-2, f). Finally, the other bands at  $\sim 880$ ,  $\sim 580$ ,  $\sim 330$ , and  $\sim 210$   $\text{cm}^{-1}$  in the spectra of all of the submonolayer catalysts in Fig. 2-1 through Fig. 2-3 are mostly unchanged, except that the  $\sim 880$   $\text{cm}^{-1}$  band in the  $\text{SnO}_2$ -promoted sample appears somewhat diminished relative to the  $\sim 880$   $\text{cm}^{-1}$  band in unpromoted 10%  $\text{WO}_3/\text{Al}_2\text{O}_3$  because of the sloping background in this spectrum.

For loadings above monolayer (1.8 monolayer-equivalents; Fig. 3-1 through Fig. 3-3), the most obvious change in the Raman spectra for samples promoted by the secondary metal oxides ( $\text{P}_2\text{O}_5$ ,  $\text{SnO}_2$ ,  $\text{Fe}_2\text{O}_3$ ,  $\text{CeO}_2$ , CaO, and  $\text{La}_2\text{O}_3$ ) is the appearance of microcrystalline compounds. The catalysts promoted with  $\text{P}_2\text{O}_5$  and  $\text{SnO}_2$ , for instance, contain small amounts of  $\text{WO}_3$  crystals (bands at 801, 713, and 268  $\text{cm}^{-1}$  [28,29]), due to slightly poorer dispersion compared to the submonolayer catalysts. Similarly,  $\alpha$ - $\text{Fe}_2\text{O}_3$  crystals (bands at 616, 495, 406, 290, and 220  $\text{cm}^{-1}$  [34]) and  $\text{CeO}_2$  crystals (band at 458  $\text{cm}^{-1}$  [33]) are present in small amounts on the samples promoted by iron oxide and ceria, respectively, for the same reason. Note that the relative Raman scattering cross-sections are much higher for oxide crystals than for the surface tungsten oxide species [30,31]. Therefore, the observed weak Raman bands due to oxide microcrystallites in the above catalysts must correspond to very small quantities of oxide crystals relative to surface tungsten oxide species.

Crystallite formation by more basic additives (CaO and  $\text{La}_2\text{O}_3$ ) at a loading of 1.8 monolayer-equivalents is due to direct interaction between the secondary metal oxide additives and the surface tungsten oxide species to create crystalline tungstate compounds. This is indicated by identical hydrated and dehydrated Raman spectra (see Ref. [35] for the dehydrated spectra of these catalysts). Unlike surface species, which readily hydrate, most crystal vibrations are unaffected by the presence of adsorbed water [28]. Specifically, in the

6%CaO/25%WO<sub>3</sub>/Al<sub>2</sub>O<sub>3</sub> catalyst (see Fig. 3-3, i), the sharp, well-defined peaks at 909, 833, 793, 387, 326, and 206 cm<sup>-1</sup> are characteristic of crystalline CaWO<sub>4</sub> [36]. These same crystalline bands also appear in the dehydrated spectra [35]. The catalyst promoted by La<sub>2</sub>O<sub>3</sub> (see Fig. 3-2, h), although lacking the same sharp, distinctive bands, also appears to form a compound with the tungsten oxide surface species at high loadings based on its very similar hydrated and dehydrated Raman spectra [35]. The spectrum of this catalyst also appears to exhibit a general change in shape relative to the unpromoted catalyst. The most likely tungstate compound formed with lanthanum oxide is La<sub>2</sub>(WO<sub>4</sub>)<sub>3</sub> (peaks at 945, 926, 726, 383, and 335 cm<sup>-1</sup> [37]).

In addition to compound formation in some of the 1.8 monolayer-equivalents catalysts, many of the highest loading catalysts also exhibit shifts in the frequency of the W=O symmetric stretch of the surface tungsten oxide species. While the addition of NiO, ZnO, and CoO to 25% WO<sub>3</sub>/Al<sub>2</sub>O<sub>3</sub> have no effect on the W=O band position (Fig. 3-1, d and Fig. 3-2, e, g), catalysts promoted by P<sub>2</sub>O<sub>5</sub>, SnO<sub>2</sub>, and Fe<sub>2</sub>O<sub>3</sub> (Fig. 3-1, a–c) display an upward shift in the W=O symmetric stretch at 975 by ~5–10 cm<sup>-1</sup>, corresponding to a shorter W=O bond

length relative to the unpromoted 25%WO<sub>3</sub>/Al<sub>2</sub>O<sub>3</sub> [15,32]. A spectral shift in the opposite direction is observed for samples promoted by CeO<sub>2</sub>, CaO, MgO, K<sub>2</sub>O, and Na<sub>2</sub>O (Fig. 3-2, f and Fig. 3-3, i–l), in which the frequency of the W=O symmetric stretch is lowered by substantial amounts (~11–18 cm<sup>-1</sup>) and implies a lengthening of the W=O bond [15,32].

In fact, the similar hydrated and dehydrated [35] spectra of catalysts promoted by K<sub>2</sub>O and Na<sub>2</sub>O at this 1.8 monolayer-equivalents loading suggest the possibility of crystalline compound formation, but the close agreement in band positions and shapes between these spectra and those of the surface tungsten oxide species in the presence of the other basic additives (oxides of Ce, Ca, and Mg) suggests that surface tungsten oxide species are present on these catalysts – not crystalline compounds. Also, the spectra of known alkali tungstates [38,39] do not match the spectra of the catalysts promoted by K<sub>2</sub>O and Na<sub>2</sub>O. Nevertheless, the surface species of K<sub>2</sub>O and Na<sub>2</sub>O clearly exert a strong influence upon the molecular structures of the surface tungsten oxide species based on the frequency shifts (18 and 15 cm<sup>-1</sup>, respectively, at a loading of 1.8 monolayer-equivalents) of the W=O symmetric stretching vibration in K<sub>2</sub>O- and

Table 3

Net surface pH at the point of zero charge (pzc) for secondary metal oxide/WO<sub>3</sub>/Al<sub>2</sub>O<sub>3</sub> catalysts

Catalyst	Net pH at pzc
10% WO <sub>3</sub> /Al <sub>2</sub> O <sub>3</sub> (0.36 monolayer coverage)	6.06
10% WO <sub>3</sub> /2.7% P <sub>2</sub> O <sub>5</sub> /Al <sub>2</sub> O <sub>3</sub> (0.7 monolayer coverage)	5.56
10% WO <sub>3</sub> /6.5% SnO <sub>2</sub> /Al <sub>2</sub> O <sub>3</sub> (0.7 monolayer coverage)	6.05
10% WO <sub>3</sub> /3.4% Fe <sub>2</sub> O <sub>3</sub> /Al <sub>2</sub> O <sub>3</sub> (0.7 monolayer coverage)	6.45
10% WO <sub>3</sub> /3.2% NiO/Al <sub>2</sub> O <sub>3</sub> (0.7 monolayer coverage)	6.54
10% WO <sub>3</sub> /3.5% ZnO/Al <sub>2</sub> O <sub>3</sub> (0.7 monolayer coverage)	6.74
10% WO <sub>3</sub> /7.4% CeO <sub>2</sub> /Al <sub>2</sub> O <sub>3</sub> (0.7 monolayer coverage)	6.80
10% WO <sub>3</sub> /3.2% CoO/Al <sub>2</sub> O <sub>3</sub> (0.7 monolayer coverage)	6.93
10% WO <sub>3</sub> /7% La <sub>2</sub> O <sub>3</sub> /Al <sub>2</sub> O <sub>3</sub> (0.7 monolayer coverage)	7.47
10% WO <sub>3</sub> /2.5% CaO/Al <sub>2</sub> O <sub>3</sub> (0.7 monolayer coverage)	7.54
10% WO <sub>3</sub> /1.7% MgO/Al <sub>2</sub> O <sub>3</sub> (0.7 monolayer coverage)	7.69
10% WO <sub>3</sub> /2% K <sub>2</sub> O/Al <sub>2</sub> O <sub>3</sub> (0.7 monolayer coverage)	8.18
10% WO <sub>3</sub> /1.3% Na <sub>2</sub> O/Al <sub>2</sub> O <sub>3</sub> (0.7 monolayer coverage)	8.32

Na<sub>2</sub>O-promoted catalysts, relative to unpromoted WO<sub>3</sub>/Al<sub>2</sub>O<sub>3</sub>.

The 1.8 monolayer-equivalents sample containing La<sub>2</sub>O<sub>3</sub> does not exhibit a separate band distinct from the symmetric stretch of the WO<sub>x</sub> units of the crystalline tungstate compound discussed previously, which means that the Raman band for the W=O symmetric stretch of the surface tungsten oxide phase is obscured in this catalyst at the highest loadings. Finally, notice from the above discussion that the majority of the secondary metal oxides (P<sub>2</sub>O<sub>5</sub>, SnO<sub>2</sub>, Fe<sub>2</sub>O<sub>3</sub>, NiO, ZnO, CoO, CeO<sub>2</sub>, MgO, K<sub>2</sub>O, and Na<sub>2</sub>O) do not form crystalline compounds with the tungsten oxide surface species, even at nearly two monolayers of total metal oxide loading (1.8 monolayer-equivalents).

### 3.2.1. Net pH at pzc measurements

The net pH at pzc experimental measurements of the 0.7 monolayer-equivalent secondary metal oxide/WO<sub>3</sub>/Al<sub>2</sub>O<sub>3</sub> catalysts are listed in Table 3. The theoretical and experimental net pH at pzc values of the bulk secondary metal oxides used in this work are presented in Table 4. Qualitatively, the net pH at pzc of the mixed metal oxide monolayer cata-

Table 4  
Net surface pH at the point of zero charge for secondary metal oxides

Metal oxide	Net pH at point of zero charge (pzc)	Ref.
WO <sub>3</sub>	0.4 (± 1.8), 0.5	[26] <sup>a</sup> , [27]
P <sub>2</sub> O <sub>5</sub>	2.9 (± 0.5)	[27] <sup>a</sup>
SnO <sub>2</sub>	4.3, 4.5	[26], [27]
CeO <sub>2</sub>	6.75	[27]
Fe <sub>2</sub> O <sub>3</sub>	8.6, 5.2–8.6	[26], [27]
ZnO	8.8, 10.3	[26], [27]
CoO	8.3 (± 2.1)	[26] <sup>a</sup>
NiO	10.3 (± 0.4)	[27]
La <sub>2</sub> O <sub>3</sub>	10.4	[27]
MgO	11, 12.4 (± 0.3)	[17], [27]
CaO	12.8 (± 0.5)	[27] <sup>a</sup>
Na <sub>2</sub> O	13.3 (± 0.5)	[27] <sup>a</sup>
K <sub>2</sub> O	13.5 (± 0.5)	[27] <sup>a</sup>

<sup>a</sup> Values calculated from formulas given in the indicated reference. (Note: The Al<sub>2</sub>O<sub>3</sub> support has a net surface pH at pzc of 8.9 [17]).

lysts correlated with the net pH at pzc of the pure bulk secondary metal oxide additives.

## 4. Discussion

### 4.1. WO<sub>3</sub>/Al<sub>2</sub>O<sub>3</sub> catalysts

The molecular structures of the hydrated surface tungsten oxide species on alumina can be determined by combining the characterization information from the present Raman spectroscopy and net pH at pzc measurements with earlier XANES studies [15]. The aqueous phase diagram for W(VI) species is shown in Fig. 4, and superimposed on this phase diagram are the tungsten oxide aqueous concentrations and net pH at pzc values of the thin aqueous film for the alumina supported tungsten oxide catalysts.

The amount of moisture present on the alumina surface under ambient conditions was determined by TGA to be approximately 8 wt% H<sub>2</sub>O [14]. There is some decrease in the amount of adsorbed moisture with increasing surface

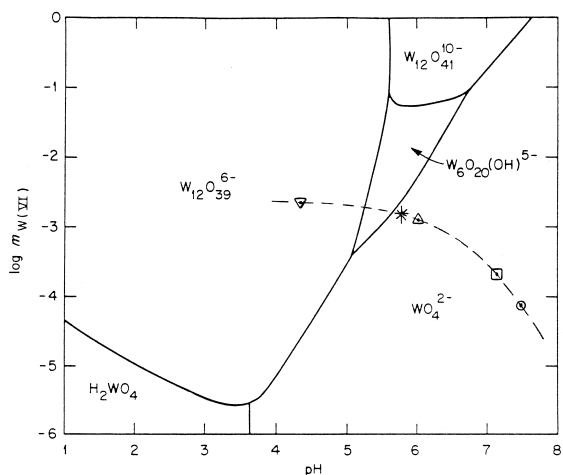


Fig. 4. Predominance diagram for aqueous W(VI) species (Ionic strength = 3 M;  $T = 50^{\circ}\text{C}$ ). Lines correspond to conditions that produce equimolar amounts of the adjacent species. The ordinate is the common logarithm of the molality of the W(VI) species. (Reprinted with permission from 'The Hydrolysis of Cations' [40]. Dashed trajectory added by the current authors based on the results of the present investigation, where the key is as follows: 1% WO<sub>3</sub>/Al<sub>2</sub>O<sub>3</sub> (O); 5% WO<sub>3</sub>/Al<sub>2</sub>O<sub>3</sub> (□); 10% WO<sub>3</sub>/Al<sub>2</sub>O<sub>3</sub> (△); 15% WO<sub>3</sub>/Al<sub>2</sub>O<sub>3</sub> (\*); and 25% WO<sub>3</sub>/Al<sub>2</sub>O<sub>3</sub> (∇).

concentration of metal oxide, but this change is small compared to the increasing content of metal oxide with loading [14]. The aqueous phase diagram suggests that the hydrated 1%  $\text{WO}_3/\text{Al}_2\text{O}_3$  catalyst should contain isolated aqueous  $\text{WO}_4^{-2}$  species. This is supported by the Raman measurements that do not show the presence of W–O–W vibrations at 580 or at  $210\text{ cm}^{-1}$ , which are characteristic of aqueous polytungstate species (see Fig. 1). The major Raman band of the isolated  $\text{WO}_4$  species is shifted from  $932$  to  $951\text{ cm}^{-1}$  due to slight distortions of this isolated species in the thin aqueous film. Comparable distortions of the isolated surface  $\text{MoO}_4$  and  $\text{ReO}_4$  species on hydrated alumina were previously also observed [41,42].

Increasing the tungsten oxide loading to 5%  $\text{WO}_3/\text{Al}_2\text{O}_3$  shifts the major Raman band from  $951$  to  $956\text{ cm}^{-1}$  and reveals the presence of W–O–W linkages by the appearance of weak bands at  $\sim 580$  and  $\sim 210\text{ cm}^{-1}$ . Thus, the 5%  $\text{WO}_3/\text{Al}_2\text{O}_3$  sample contains some paratungstate-A species,  $\text{HW}_6\text{O}_{21}^{-5}$ , in addition to the monotungstate species. The presence of paratungstate-B, with bands at  $955$  and  $880\text{ cm}^{-1}$  (see Table 1) cannot be ruled out based solely on the Raman spectra. However, its formation is quite unlikely based on the phase diagram in Fig. 4, which shows that the trajectory for the samples under study never comes near the region of paratungstate-B,  $\text{HW}_{12}\text{O}_{42}^{-10}$ , located in the upper right corner of the figure. The aqueous phase diagram further suggests that the 10 and 15%  $\text{WO}_3/\text{Al}_2\text{O}_3$  samples are in the region where both isolated  $\text{WO}_4^{-2}$  and paratungstate-A ( $\text{HW}_6\text{O}_{21}^{-5}$ ) should coexist, but should be dominated by the isolated species. Note that the lines in the aqueous phase diagram represent conditions under which equal amounts of the species in adjacent regions are present. XANES measurements confirm that the hydrated surface tungsten oxide species on alumina at these concentrations is predominantly tetrahedrally coordinated [15], and Raman reveals the presence of the polytungstate species

by the appearance of the W–O–W vibrations (see Fig. 1). The presence of the paratungstate-A,  $\text{HW}_6\text{O}_{21}^{-5}$ , species shifts the major Raman band to  $966$ – $967\text{ cm}^{-1}$ .

The aqueous phase diagram suggests that the 25%  $\text{WO}_3/\text{Al}_2\text{O}_3$  sample should predominantly contain octahedrally coordinated metatungstate species. This is supported by XANES measurements which reveal that the octahedral coordination is predominant for high loadings of hydrated  $\text{WO}_3/\text{Al}_2\text{O}_3$  catalysts [15]. The major Raman peak shifts to  $975\text{ cm}^{-1}$ , which is consistent with the U-metatungstate species since both metatungstate ( $\text{H}_2\text{W}_{12}\text{O}_{40}^{-6}$ ) and polytungstate-Y ( $\text{W}_{10}\text{O}_{32}^{-4}$ ) would possess two strong Raman bands in the  $960$ – $990\text{ cm}^{-1}$  region (see Table 1). Furthermore, both the  $\text{H}_2\text{W}_{12}\text{O}_{40}^{-6}$  and  $\text{W}_{10}\text{O}_{32}^{-4}$  species exist in the pH range of 1–3, which is below the net pH at pzc for the  $\text{WO}_3/\text{Al}_2\text{O}_3$  catalysts (see Table 2). Thus, the characterization studies demonstrate that the hydrated surface tungsten oxide overlayer on alumina possesses  $\text{WO}_4^{-2}$ ,  $\text{HW}_6\text{O}_{21}^{-5}$ , and U-metatungstate species and that their relative concentrations are a function of surface coverage and the net surface pH at pzc of the hydrated layer.

The molecular structures of the hydrated surface tungsten oxide species on alumina have recently also been examined by proton affinity measurements and TEM [43,44]. The proton affinity measurements confirmed that the surface tungsten oxide species on alumina was not crystalline  $\text{WO}_3$ , but that it was present as hydrated paratungstate and metatungstate species. The TEM measurements of a series of  $\text{WO}_3/\text{Al}_2\text{O}_3$  catalysts revealed the presence of tungsten oxide clusters about  $5$ – $8\text{ \AA}$  in size, which is consistent with the presence of  $\text{HW}_6\text{O}_{21}^{-5}$  and metatungstate clusters at about pH 1–6. Unfortunately, TEM is not capable of discriminating between these different polytungstate species and does not have the resolution to detect the isolated  $\text{WO}_4^{-2}$  aqueous species. Although XANES can discriminate among octahedrally and tetrahedrally coordi-

nated tungstates, it is not capable of discriminating among the several different octahedral polytungstate species that can be present in hydrated samples [15,45]. The current Raman study reveals that several of these aqueous tungsten oxide complexes can simultaneously exist on the alumina support surface and that molecular spectroscopies that can discriminate among all the species are required to fully characterize the hydrated alumina supported metal oxide species present on the catalyst. Similar Raman bands were also observed on other ambient supported tungsten oxide catalysts, indicating that the same aqueous species are also present on other oxide supports [17,46,47].

#### 4.2. Secondary metal oxide / 10% $WO_3/Al_2O_3$ catalysts (0.7 monolayer coverage)

The addition of secondary metal oxide additives to the 10%  $WO_3/Al_2O_3$  catalysts primarily resulted in the formation of surface metal oxide species rather than mixed tungsten oxide crystalline compounds because of the strong interaction between these oxides and the alumina support surface (during catalyst calcination when the surface is dehydrated). The absence of strong crystalline Raman bands, with the exception of  $CeO_2$  and  $La_2(WO_4)_3$  crystals, as well as the presence of spectral changes upon dehydration of the catalysts [35], confirm that crystalline compounds were absent from these mixed metal oxide monolayer catalysts containing 0.7 monolayer coverage. The same correlation between the molecular structure of the tungsten oxide surface species and the net pH at pzc which applied to unpromoted  $WO_3/Al_2O_3$  catalysts also appears to apply to the promoted catalysts. Furthermore, the secondary metal oxides affect the structures of the hydrolyzed mono- and isopolytungstates, the species which dominate the Raman spectra, by changing the net pH at pzc of the thin aqueous film on the catalyst surface.

Comparison of the Raman spectra, Fig. 2-1 through Fig. 2-3, with the corresponding net pH

at pzc measurements, Table 3, reveals a systematic trend for the influence of the secondary metal oxide additives upon the molecular structures of the hydrated surface tungsten oxide species on alumina. The metal oxide additives (oxides of P, Sn, and Fe) that did not significantly perturb the net pH at pzc relative to unpromoted  $WO_3/Al_2O_3$ , in the pH region of approximately 5.5 to 6.5, also did not appear to perturb the hydrated surface tungsten oxide species on alumina. These hydrated samples possessed Raman bands in the 962–967  $cm^{-1}$  region which are associated with the presence of isolated  $WO_4^{-2}$  and polytungstate  $HW_6O_{21}^{-5}$  aqueous species, with the isolated species being the predominant species according to the XANES studies mentioned above.

The metal oxide additives (oxides of Ni, Zn, Ce, Co, Ca, Mg, K, and Na) increased the net pH at pzc values from approximately 6.5 to 8.4 and decreased the positions of the Raman bands of the hydrated surface tungsten oxide species to 952–961  $cm^{-1}$ . These changes are associated with an increase in the ratio of  $WO_4^{-2}$  to  $HW_6O_{21}^{-5}$  aqueous species. The presence of some polytungstate species in these samples is confirmed by the observation of W–O–W linkages in the Raman spectra (see Fig. 2-1 through Fig. 2-3). An exception to the samples with the net pH at pzc in the 6.5 to 8.4 range is the lanthanum oxide promoted  $WO_3/Al_2O_3$  catalyst. A strong acid–base reaction between the tungsten and lanthanum oxides is believed to be responsible for the formation of insoluble  $La_2(WO_4)_3$ .

The correlation between the tungsten oxide molecular structure and the net pH at pzc on the catalyst surface does not support the concept of a direct interaction of the secondary metal oxide additives with the hydrated surface tungsten oxide species on alumina at submonolayer coverages. This appears to be true for both negatively charged (oxides of P and Sn) and positively charged (oxides of Fe, Ni, Zn, Ce, Co, Ca, Mg, K and Na) precursors. Instead, at submonolayer coverages, the secondary metal ox-

ide additives are primarily present as hydrated surface metal oxide species, influencing the structure of the hydrated surface tungsten oxide species on alumina indirectly by altering the net pH at pzc of the aqueous thin film on the catalyst surface.

Some conflicting data have been offered by Schwarz et al. [43,44,48], who find evidence from temperature programmed reduction, X-ray diffraction, and oxidation activity studies for the presence of Ni–W [48] and Co–W [44] interaction species on  $\text{WO}_3/\text{Al}_2\text{O}_3$ . Schwarz et al. propose  $\text{Co}_2\text{W}_{12}\text{O}_{42}^{-8}$ , a heteropolyanion with the Keggin structure, and  $\text{NiWO}_4$  as the most likely interaction species. However,  $\text{NiWO}_4$  is not detected in any of the  $\text{NiO}/\text{WO}_3/\text{Al}_2\text{O}_3$  Raman spectra. Likewise,  $\text{Co}_2\text{W}_{12}\text{O}_{42}^{-8}$  is unlikely to form at submonolayer loadings, since the net pH at pzc of these samples ( $> 5.5$ , Table 3, after calcination and rehydration under ambient conditions), is probably too high to allow formation of heteropolyanions, which usually form only in very acidic solutions [25]. For these hydrated catalysts, the possibility of heteropolytungstates cannot be absolutely ruled out, since they are expected to give Raman spectra comparable to the structurally similar metatungstate isopolyanion [49], but no significant Ni–W or Co–W interactions are detected in the dehydrated Raman data [35].

#### 4.3. Secondary metal oxide / 25% $\text{WO}_3/\text{Al}_2\text{O}_3$ catalysts (1.8 monolayer coverage)

The addition of secondary metal oxide additives to the 25%  $\text{WO}_3/\text{Al}_2\text{O}_3$  catalysts resulted in the formation of both surface metal oxide species, and, for some systems, mixed tungsten oxide crystalline compounds. Surprisingly, for most of the mixed metal oxide monolayer systems the alumina support was able to accommodate approximately two monolayer-equivalents of the surface metal oxides (oxides of P, Sn, Fe, Ni, Zn, Co, Ce, Mg, K and Na) without the significant formation of crystalline phases. The absence of strong crystalline bands, especially

at such high loadings, suggests that strong interaction exists between the metal oxides and the alumina support (during catalyst calcination when the surface is dehydrated). More importantly, this ability of the alumina surface to prevent crystalline tungstate formation well above monolayer coverage strongly implies that many of the secondary surface metal oxide species occupy different sites on the alumina support than the surface tungsten oxide species. The surface tungsten oxide species primarily anchor to the dehydrated alumina support by titrating the surface hydroxyls [50], but many of the secondary metal oxide additives interact directly with the defects in the dehydrated alumina support (coordinately unsaturated  $\text{Al}^{+3}$  Lewis acid sites) [51].

The formation of crystalline mixed tungsten oxide compounds, which were found between the surface tungsten oxide species and some of the more basic secondary metal oxides ( $\text{CaWO}_4$  and  $\text{La}_2(\text{WO}_4)_3$ ), is attributed to an acid–base reaction between the secondary metal oxides and the tungsten oxide. Apparently, the preferential interaction of the tungsten oxide and secondary metal oxides with the alumina support is not as great at high loadings as it was below monolayer coverage. However, the presence of tungsten oxide surface species in coexistence with these compounds at 1.8 monolayer-equivalents suggests that a large portion of the deposited metal oxides are still preferentially interacting with the alumina. Therefore, it is most likely that these high loadings of metal oxides exceed the number of available alumina surface sites, forcing the metal oxides to interact with each other during calcination (when the catalyst surface is dehydrated) instead of interacting with the alumina surface.

Despite compound formation in some catalysts, the molecular structures of the hydrated surface tungsten oxide species on alumina above monolayer coverage (1.8 monolayer-equivalents) appear to follow the same trend with the net pH at pzc of the secondary metal oxide additives as observed above for samples con-

taining submonolayer coverages. However, the net pH at pzc values were not measured for this series of catalysts. The 25%  $\text{WO}_3/\text{Al}_2\text{O}_3$  catalyst exhibited a Raman band at  $975\text{ cm}^{-1}$  which was earlier assigned to U-metatungstate species. Addition of oxides of P, Sn and Fe shifted the Raman band of the surface tungsten oxide species to  $981\text{--}984\text{ cm}^{-1}$ , which may be due to the presence of some  $\text{H}_2\text{W}_{12}\text{O}_{40}^{-6}$  or  $\text{W}_{10}\text{O}_{32}^{-4}$  aqueous species that exist at aqueous pH values of approximately 1–3. It might also be possible, in this particular case, to form a heteropolytungstate, such as  $\text{PW}_{12}\text{O}_{40}^{-3}$ , since the acidity of the thin aqueous film is quite high. However, it is impossible to distinguish between this heteropolytungstate ion and the metatungstate ion with Raman spectroscopy because the two ions have the same symmetry and Keggin structure [49].

Lastly, recall that the Raman bands of the  $\text{WO}_3/\text{Al}_2\text{O}_3$  catalyst were not altered by the addition of oxides of Ni, Zn, and Co, which suggests that these samples possess the U-metatungstate aqueous clusters which exist at aqueous pH values of approximately 3–5. Addition of oxides of Ce, Ca, Mg, K, and Na shifted the Raman band of the surface tungsten oxide species to  $957\text{--}964\text{ cm}^{-1}$ , which suggests the presence of both  $\text{WO}_4^{-2}$  and  $\text{HW}_6\text{O}_{21}^{-5}$  aqueous species for these catalysts (typically present at aqueous pH values of approximately 5–8). Thus, even above monolayer coverage, the surface metal oxide additives affect the molecular structures of the hydrated surface tungsten oxide species on alumina by influencing the net pH at pzc of the thin aqueous film on the support.

## 5. Conclusions

Raman characterization studies revealed that the hydrated surface tungsten oxide overlayer on alumina possesses  $\text{WO}_4^{-2}$ ,  $\text{HW}_6\text{O}_{21}^{-5}$  and U-metatungstate species and that their relative concentrations are a function of surface cover-

age and the net pH at pzc of the hydrated layer. The monotungstate ion predominates at high pH, but low pH values favor the formation of the polytungstates. At submonolayer coverages, the addition of secondary metal oxides to the 10%  $\text{WO}_3/\text{Al}_2\text{O}_3$  catalyst primarily resulted in the formation of surface metal oxide species rather than mixed tungsten oxide crystalline compounds because of the preferential interaction of the metal oxides with the alumina support surface during the calcination treatment. Furthermore, the secondary metal oxide additives did not interact directly with the tungsten oxide surface species, but instead interacted only indirectly by altering the net pH at pzc of the thin aqueous film on the catalyst surface.

Above monolayer coverages, addition of secondary metal oxides to the 25%  $\text{WO}_3/\text{Al}_2\text{O}_3$  catalyst resulted both in the formation of surface metal oxide species and mixed tungsten oxide crystalline compounds. The systems that tended to form mixed tungsten oxide crystalline compounds generally possessed the more basic metal oxide additives (Ca, La). In the absence of mixed tungsten oxide compound formation, the alumina support was able to accommodate approximately two monolayer-equivalents of the surface metal oxide species, which suggests that tungsten oxide and the secondary metal oxide additives occupy different surface sites on the alumina support during calcination. The surface tungsten oxide species preferentially interact with the alumina surface hydroxyls and the secondary metal oxide additives preferentially interact with the coordinately unsaturated  $\text{Al}^{+3}$  Lewis acid sites. The molecular structures of the hydrated surface tungsten oxide species on alumina above monolayer coverage appeared to follow the same trend with the net pH at pzc of the secondary metal oxide additives as observed for submonolayer coverages. The current investigation demonstrates that Raman spectroscopy is able to follow the structural changes of hydrated surface tungsten oxide species on alumina as a function of surface coverage and in the presence of secondary metal oxide additives.

## Acknowledgements

This work was supported by the U.S. Department of Energy under grants DEFG02-93ER14350 (Lehigh University) and DEFG05-86ER13604 (University of Texas at Austin).

## References

- [1] L.L. Murrell, C.J. Kim, D.C. Grenoble, U.S. Pat. No. 4,233,139, 1980.
- [2] D.C. Grenoble, C.J. Kim, L.L. Murrell, U.S. Pat. No. 4,440,872, 1984.
- [3] J. Berholc, J.A. Horsley, L.L. Murrell, L.G. Sherman, S. Soled, *J. Phys. Chem.* 91 (1987) 1526.
- [4] L.L. Murrell, D.C. Grenoble, C.J. Kim, N.C. Dispenziere, *J. Catal.* 107 (1987) 463.
- [5] C. Wivel, B.S. Clausen, R. Candia, S. Morup, H. Topsøe, *J. Catal.* 87 (1984) 497.
- [6] H. Knozinger, *Proc. 9th Intern. Congr. Catalysis*, vol. 5, 1988, p. 20.
- [7] F.T. Clark, A.L. Hensley, J.Z. Shyu, J.A. Kaduk, G.J. Ray, in: J.B. Butt, C.H. Bartholomew (Eds.), *Catalyst Deactivation 1991*, vol. 68, Elsevier Science Publishers, Amsterdam, 1991, p. 417.
- [8] F.T. Clark, A.L. Hensley, U.S. Pat. No. 4,994,423, 1991.
- [9] F.T. Clark, A.L. Hensley, U.S. Pat. No. 4,997,799, 1991.
- [10] F.T. Clark, A.L. Hensley, U.S. Pat. No. 5,071,538, 1991.
- [11] M.A. Vuurman, Ph.D. thesis, University of Amsterdam, 1992.
- [12] J.M. Stencel, *Raman Spectroscopy for Catalysis*, Van Nostrand Reinhold, New York, 1990.
- [13] I.E. Wachs, F.D. Hardcastle, in: *Catalysis*, vol. 10, Royal Society of Chemistry, Cambridge, U.K., 1993, pp. 102–153.
- [14] S.D. Kohler, J.G. Ekerdt, D.S. Kim, I.E. Wachs, *Catal. Lett.* 16 (1992) 231.
- [15] J.A. Horsley, I.E. Wachs, J.M. Brown, G.H. Via, F.D. Hardcastle, *J. Phys. Chem.* 91 (1987) 4014.
- [16] M.A. Vuurman, I.E. Wachs, *J. Phys. Chem.* 96 (1992) 5008.
- [17] G. Deo, I.E. Wachs, *J. Phys. Chem.* 95 (1991) 5889.
- [18] K.H. Tytko, B. Schonfeld, V. Cordis, O. Glemser, Presented at the 15th Int. Conf. Coord. Chem., 1973, partly published in: *Z. Naturforsch. B*, 30 (1975) 471 and in *Z. Naturforsch. B*, 30 (1975) 834.
- [19] K.Y. Simon Ng, E. Gulari, *Polyhedron* 3 (1984) 1001.
- [20] W.P. Griffith, J.B. Lesniak., *J. Chem. Soc. A*, (1969) 1066.
- [21] C. Baes, R.E. Mesmer, *The Hydrolysis of Cations*, John Wiley and Sons, New York, 1976, p. 258.
- [22] K.H. Tytko, O. Glemser, in: H.J. Emeleus, A.G. Sharpe (Eds.), *Advances in Inorganic Chemistry and Radiochemistry*, vol. 19, Academic Press, New York, 1976, p. 239, 280.
- [23] D.L. Kepert, in: F.A. Cotton (Ed.), *Progress in Inorganic Chemistry*, vol.4, John Wiley and Sons, New York, 1962, p. 199.
- [24] W.P. Griffith, T.D. Wickins, *J. Chem. Soc. A*, (1967) 675.
- [25] C.L. Rollinson, in: A.F. Trotman-Dickenson (Ed.), *Comprehensive Inorganic Chemistry*, Pergamon Press, Oxford, UK, vol. 3, 1973, pp. 766–768.
- [26] M.A. Butler, D.S. Ginley, *J. Electrochem. Soc.* 125 (1978) 228.
- [27] G. Parks, *Chem. Rev.* 65 (1965) 177.
- [28] I.E. Wachs, F.D. Hardcastle, S.S. Chan, *Spectrosc.* 1 (1986) 30.
- [29] D.S. Kim, M.M. Ostromecki, I.E. Wachs, *J. Mol. Catal. A* 106 (1996) 93.
- [30] S.S. Chan, I.E. Wachs, L.L. Murrell, *J. Catal.* 90 (1984) 150.
- [31] S.S. Chan, I.E. Wachs, *J. Catal.* 103 (1987) 224.
- [32] F.D. Hardcastle, I.E. Wachs, *J. Raman Spectrosc.* 26 (1995) 397.
- [33] J.Z. Shyu, W.H. Weber, H.S. Gandhi, *J. Phys. Chem.* 92 (1988) 4964.
- [34] M.A. Vuurman, I.E. Wachs, *J. Mol. Catal.* 77 (1992) 29.
- [35] M.M. Ostromecki, L.J. Burcham, I.E. Wachs, *J. Mol. Catal. A* 132 (1998) 59.
- [36] J.P. Russell, R. Loudon, *Proc. Phys. Soc.* 85 (1965) 1029.
- [37] L.J. Burcham, I.E. Wachs, *Spectrochim. Acta Part A*, (1997), submitted for publication.
- [38] H.J. Becher, *J. Less-Common Metals* 76 (1980) 169.
- [39] F. Knee, R.A. Condrate Sr., *J. Phys. Chem. Solids.* 40 (1979) 1145.
- [40] C. Baes, R. Mesmer (Eds.), *The Hydrolysis of Cations*, John Wiley and Sons, New York, 1976, p. 258.
- [41] H. Hu, I.E. Wachs, S.R. Bare, *J. Phys. Chem.* 99 (1995) 10897.
- [42] M.A. Vuurman, D.J. Stufkens, A. Oskam, I.E. Wachs, *J. Mol. Catal.* 76 (1992) 263.
- [43] C. Contescu, J. Jagiello, J.A. Schwarz, *J. Phys. Chem.* 97 (1993) 10152.
- [44] R. Zhang, J.A. Schwarz, A. Datye, J.P. Baltrus, *J. Catal.* 135 (1992) 200.
- [45] F. Hilbrig, H.E. Gobel, H. Knozinger, H. Schmelz, B. Lengeler, *J. Phys. Chem.* 95 (1991) 6973.
- [46] M.A. Vuurman, I.E. Wachs, A.M. Hirt, *J. Phys. Chem.* 95 (1991) 9928.
- [47] D.S. Kim, M. Ostromecki, I.E. Wachs, S.D. Kohler, J.G. Ekerdt, *Catal. Lett.* 33 (1995) 209.
- [48] D.W. Southmayd, C. Contescu, J.A. Schwarz, *J. Chem. Soc. Faraday Trans.* 89 (1993) 2075.
- [49] A.F. Wells, *Structural Inorganic Chemistry*, 5th ed., Oxford University Press, Oxford, UK, 1984, p. 523.
- [50] A.M. Turek, I.E. Wachs, E. DeCanio, *J. Phys. Chem.* 96 (1992) 5000.
- [51] M.A. Vuurman, D.J. Stufkens, A. Oskam, G. Deo, I.E. Wachs, *J. Chem. Soc. Farad. Trans.* 92 (1996) 3259.